

Baryon Stopping as a Probe of Deconfinement Onset in Relativistic Heavy-Ion Collisions

Yu.B. Ivanov^{1,*}

¹*Kurchatov Institute, Moscow RU-123182, Russia*

It is argued that an irregularity in the baryon stopping is a natural consequence of a phase transition occurring in the compression stage of a nuclear collision. It is a combined effect of the softest point inherent in an equation of state (EoS) with a phase transition and a change in the nonequilibrium dynamics from hadronic to partonic transport. Thus, this irregularity is a signal from a hot and dense stage of the nuclear collision. In order to illustrate this proposition, calculations within the three-fluid model were performed with three different EoS's: a purely hadronic EoS, an EoS with a first-order phase transition and that with a smooth crossover transition. It is found that predictions within the first-order-transition scenario indeed reveal an a strong irregularity in the incident energy dependence of the form of the net-proton rapidity distributions in central collisions. This behavior is in contrast to that for the hadronic scenario, where the distribution form gradually evolve, displaying no irregularity. The case of the crossover EoS is intermediate. Only a weak irregularity takes place. Experimental data also exhibit a trend of similar irregularity, which is however based on still preliminary data at energies of 20A GeV and 30A GeV.

PACS numbers: 25.75.-q, 25.75.Nq, 24.10.Nz

Keywords: relativistic heavy-ion collisions, baryon stopping, hydrodynamics, phase transition

I. INTRODUCTION

Onset of deconfinement in relativistic heavy-ion collisions is now in focus of theoretical and experimental studies of relativistic heavy-ion collisions. This problem is one of the main motivations for the currently running beam-energy scan [1] at the Relativistic Heavy-Ion Collider (RHIC) at Brookhaven National Laboratory (BNL) and low-energy-scan program [2] at Super Proton Synchrotron (SPS) of the European Organization for Nuclear Research (CERN), as well as newly constructed Facility for Antiproton and Ion Research (FAIR) in Darmstadt [3] and the Nuclotron-based Ion Collider Facility (NICA) in Dubna [4]. In this paper I would like to argue that the baryon stopping in nuclear collision can be a sensitive probe of the deconfinement onset.

In fact, an irregularity in the incident-energy dependence of the baryon stopping is very natural if the system undergoes a phase transition. Let us start with discussion of the conventional (i.e. one-fluid) hydrodynamics, which is applied to the whole process of the nuclear collision, e.g. from its compression stage to the expansion stage up to freeze-out, like it is done in Refs. [5, 6].

The form of the resulting rapidity distribution of net-baryons depends on the spatial form of the produced fireball. If the fireball is almost spherical, the expansion of the fireball is essentially 3-dimensional which results in a peak at the midrapidity in the rapidity distribution. This statement is a theorem that can be proved in few lines. If a the fireball is strongly deformed (compressed) in the beam direction, i.e. has a form of a disk, its expansion is approximately 1-dimensional that produces a dip at

the midrapidity, which is confirmed by numerous simulations, see e.g. Ref. [7]. In terms of the fluid mechanics this is a consequence of interaction of two rarefaction waves propagating from opposite peripheral sides of decaying disk toward its center [8]. This speculation is very similar to that related to the elliptic flow: a strong elliptic flow results from a strongly deformed almond-shaped initial fireball with the deformation of the resulting momentum distribution of particles being inverse to the spatial deformation of the initial fireball. The physical mechanism here is precisely the same, only the expansion is developed in the transverse direction.

The next question is how this fireball is formed. This is already a matter of dynamics in the early compression stage of the nuclear collision. A softest point [9] characteristic of EoS's with a phase transition plays an important role in this compression dynamics. At low energies the softest point is not reached in the collision process, the system remains stiff and therefore the produced fireball is almost spherical. As a result, the baryon rapidity distribution is peaked at the midrapidity. When the incident energy gets high enough, the softest-point region of the EoS starts to dominate during the compression stage, the system weaker resists to the compression and hence the resulting fireball becomes more deformed, i.e. more of the disk shape. Then its expansion is close to the 1-dimensional pattern and, as a result, we have a dip at the midrapidity. With energy rise, the stiffness of the EoS (in the range relevant to compression stage) grows, the system stats to be more resistant to the compression and hence the produced fireball becomes less deformed. The expansion of this fireball results in a peak or, at least, to a weaker dip at the midrapidity as compared to that at the “softest-point” incident energy. With further energy rise, the initial kinetic pressure overcomes the stiffness of the EoS and makes the produced fireball strongly de-

*e-mail: Y.Ivanov@gsi.de

formed again, which in its turn again results in a dip at the midrapidity.

Thus, even without any nonequilibrium, we can expect a kind of a “peak-dip-peak-dip” irregularity in the incident energy dependence of the form of the net-proton rapidity distributions. Nonequilibrium also contributes to this irregularity. At a phase transformation¹ the hadronic degrees of freedom are changed to partonic ones. In particular, it means a change in cross sections which govern the nuclear stopping power. Therefore, this change also induces a certain irregularity in the stopping power. Only the dip at the midrapidity in ultrarelativistic nuclear collisions has a different origin in the actual case of weak baryon stopping as compared with that in the conventional hydrodynamics. It occurs because the baryon charges of colliding nuclei traverse through each other.

It is important to emphasize that the “peak-dip-peak-dip” irregularity is a signal from the hot and dense stage of the nuclear collision.

In the present paper this qualitative pattern is illustrated by calculations within a model of the three-fluid dynamics (3FD) [10] employing three different equations of state (EoS): a purely hadronic EoS [11] (hadr. EoS), which was used in the major part of the 3FD simulations so far [10, 12–15], and two versions of EoS involving the deconfinement phase transition [16]. These two versions are an EoS with the first-order phase transition (2-phase EoS) and that with a smooth crossover transition (crossover EoS). The softest points in these EoS’s are illustrated in Ref. [17]. The hadronic EOS [11] possesses no softest point - stiffness of the EoS changes monotonously. Preliminary results of simulations with phase transitions have been already reported in Refs. [18, 19]. Here I present calculations with thoroughly tuned friction forces in the quark-gluon phase, which made it possible to reasonably reproduce a great number of observables in the incident energy range $2.7 \text{ GeV} \leq \sqrt{s_{NN}} \leq 62.4 \text{ GeV}$ in terms of the center-of-mass energy. Details of this calculations and results on a great number of bulk observables (rapidity and transverse spectra, flow observables and multiplicities) for various species and a large number of incident energies, their comparison with available data will be reported elsewhere. Here I would like to focus on rapidity distributions of net-protons in central collisions of heavy nuclei in the AGS-SPS energy range. The distribution of net-protons is the best probe of the nuclear stopping in the absence of data on net-baryons.

Concerning the fit of the friction force, few comments are in order. The friction in the hadronic phase was estimated in Ref. [20]. Within hadronic scenario (hadr. EoS) we had to enhance this friction in order to repro-

duce the baryon stopping at high energies [10]. Though such a enhancement is admissible in view of uncertainties of the estimated friction, the value of the enhancement looks too high. Indeed, at $\sqrt{s_{NN}} = 17.3 \text{ GeV}$, i.e. at the top SPS energy, this enhancement exceeds the factor of 2. In scenarios with phase transitions there is no need to modify the hadronic friction. This can be considered as a theoretical argument in favor of such scenarios.

II. EQUATIONS OF STATE

The 2-phase and crossover EoS’s still differ even at very high densities. The latter means that the crossover transition constructed in Ref. [16] is very smooth. The hadronic fraction survives up to very high densities. In particular, this is seen from Fig. 1: the fraction of the quark-gluon phase (W_{QGP}) reaches value of 0.5 only at very high energy densities. In this respect, this version of the crossover EoS certainly contradicts results of the lattice QCD calculations, where a fast crossover, at least at zero chemical potential, was found [21]. Therefore, a true EoS is somewhere in between the crossover and 2-phase EoS’s of Ref. [16].

Figure 1 demonstrates that the onset of the phase transition in the calculations happens at top-AGS–low-SPS energies. Similarly to Ref. [22], the figure displays dynamical trajectories of the matter in a central box placed around the origin $\mathbf{r} = (0, 0, 0)$ in the frame of equal velocities of colliding nuclei: $|x| \leq 2 \text{ fm}$, $|y| \leq 2 \text{ fm}$ and $|z| \leq \gamma_{cm} 2 \text{ fm}$, where γ_{cm} is Lorentz factor associated with the initial nuclear motion in the c.m. frame. Initially, the colliding nuclei are placed symmetrically with respect to the origin $\mathbf{r} = (0, 0, 0)$, z is the direction of the beam. At a given density n_B , the zero-temperature compressional energy, $\varepsilon(n_B, T = 0)$, provides a lower bound on the energy density ε , so the accessible region is correspondingly limited. In the case of the crossover EoS only the region of the mixed phase between $W_{QGP} = 0.1$ and $W_{QGP} = 0.5$ is displayed, since in fact the mixed phase occupies the whole (ε, n_B) region. The ε, n_B representation is chosen because these densities are dynamical quantities and, therefore, are suitable to compare calculations with different EoS’s.

Only expansion stages of the evolution are displayed, where the matter in the box is already thermally equilibrated. Evolution proceeds from the top point of the trajectory downwards. Subtraction of the $m_N n_B$ term is taken for the sake of suitable representation of the plot. The size of the box was chosen to be large enough that the amount of matter in it can be representative to conclude on the onset of the phase transition and to be small enough to consider the matter in it as a homogeneous medium. Nevertheless, the matter in the box still amounts to a minor part of the total matter of colliding nuclei. Therefore, only the minor part of the total matter undergoes the phase transition at 10A GeV energy.

As seen, the phase transition starts at the top AGS en-

¹ The term “phase transition” is deliberately avoided, since it usually implies thermal equilibrium.

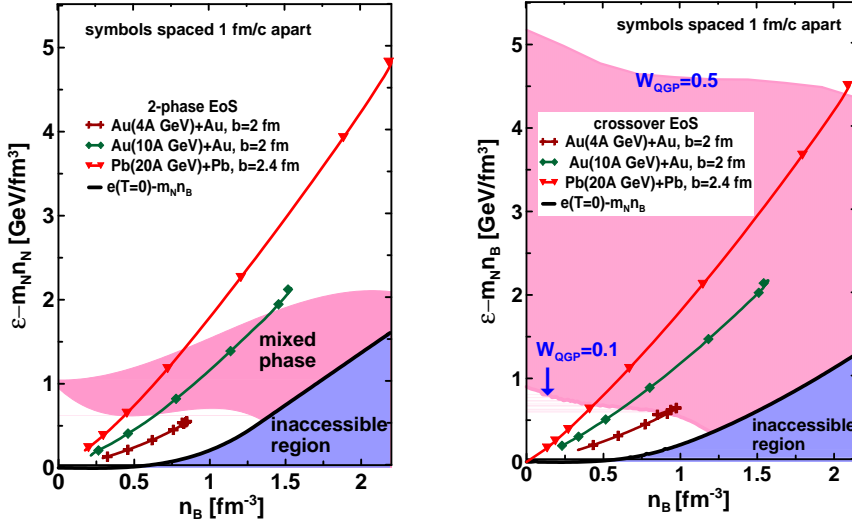


FIG. 1: Dynamical trajectories of the matter in the central box of the colliding nuclei ($4\text{fm} \times 4\text{fm} \times \gamma_{cm}4\text{fm}$), where γ_{cm} is the Lorentz factor associated with the initial nuclear motion in the c.m. frame, for central ($b = 2$ fm) collisions of Au+Au at 4A and 10A GeV energies and Pb+Pb at 20A GeV. The trajectories are plotted in terms of baryon density (n_B) and the energy density minus n_B multiplied by the nucleon mass ($\varepsilon - m_N n_B$). Only expansion stages of the evolution are displayed. The trajectories are presented for two EoS's: 2-phase EoS (left panel) and crossover EoS (right panel). Symbols on the trajectories indicate the time rate of the evolution: time span between marks is 1 fm/c. For the 2-phase EoS (left panel) the shadowed “mixed phase” region is located between the borders, where the QGP phase start to raise ($W_{QGP} = 0$) and becomes completely formed ($W_{QGP} = 1$). For the crossover EoS (right panel) the corresponding borders correspond to values of the QGP fraction $W_{QGP} = 0.1$ and $W_{QGP} = 0.5$. Inaccessible region is restricted by $\varepsilon(n_B, T = 0) - m_N n_B$ from above.

ergies in both cases. It gets practically completed at low SPS energies in the case of the case of the 2-phase EoS. In the crossover scenario it lasts till very high incident energies. The trajectories for two different EoS's are nevertheless very similar at displayed energies. Apparently, it happens because the friction in the quark-gluon phase was selected in such a way that both scenarios reasonably reproduce available data at high energies.

III. PROTON AND NET-PROTON RAPIDITY DISTRIBUTIONS

A direct measure of the baryon stopping is the net-baryon (i.e. baryons-minus-antibaryons) rapidity distribution. However, since experimental information on neutrons is unavailable, we have to rely on net-proton (i.e. proton-minus-antiproton) data. Presently there exist experimental data on proton (or net-proton) rapidity spectra at AGS [23–26] and SPS [27–30] energies. These data were analyzed within various models [5, 6, 10, 12, 33–39].

Figure 2 presents calculated rapidity distributions of protons (for AGS energies) and net-protons (for SPS energies) and their comparison with available data. Notice that difference between protons and net-protons, as well as a contribution of weak decays to these yields are negligible at the AGS energies, see compilation of experimental data in Ref. [40]. Contribution of weak decays of strange

hyperons into proton yield was disregarded in accordance with measurement conditions of the NA49 collaboration. Correspondence between the fraction of the total cross section related to a data set and a mean value of the impact parameter was read off from the paper [32] in case of NA49 data. For Au+Au collisions it was approximately estimated proceeding from geometrical considerations.

As seen from Fig. 2, at lower AGS energies all EoS's predict the same results, since at these energies only hadronic parts of all EoS's are relevant, see Fig. 1. Results of the 2-phase EoS start to differ from those of the hadr. and crossover EoS's beginning from 6A GeV: the 2-ph.-EoS distributions reveal a dip at the midrapidity. This dip contradicts the available experimental data and is very robust: variation of the friction in a wide range does not remove this dip. Therefore, it is a direct consequence of the onset of the first-order phase transition, which starts precisely at these energies in the 2-ph.-EoS scenario, see Fig. 1. This dip survives even in one-fluid calculations [5, 6] involving the 1st-order phase transition in spite of immediate baryon stopping inherent in the one-fluid model. In 3FD calculations, this dip changes into midrapidity peak at higher energies (30A GeV and 40A GeV). With further energy rise ($E_{lab} > 40A$ GeV) the midrapidity peak again transforms into a dip, see also Fig. 2. The latter dip is already a normal behavior which takes place at arbitrary high energies.

The experimental distributions exhibit a qualitatively

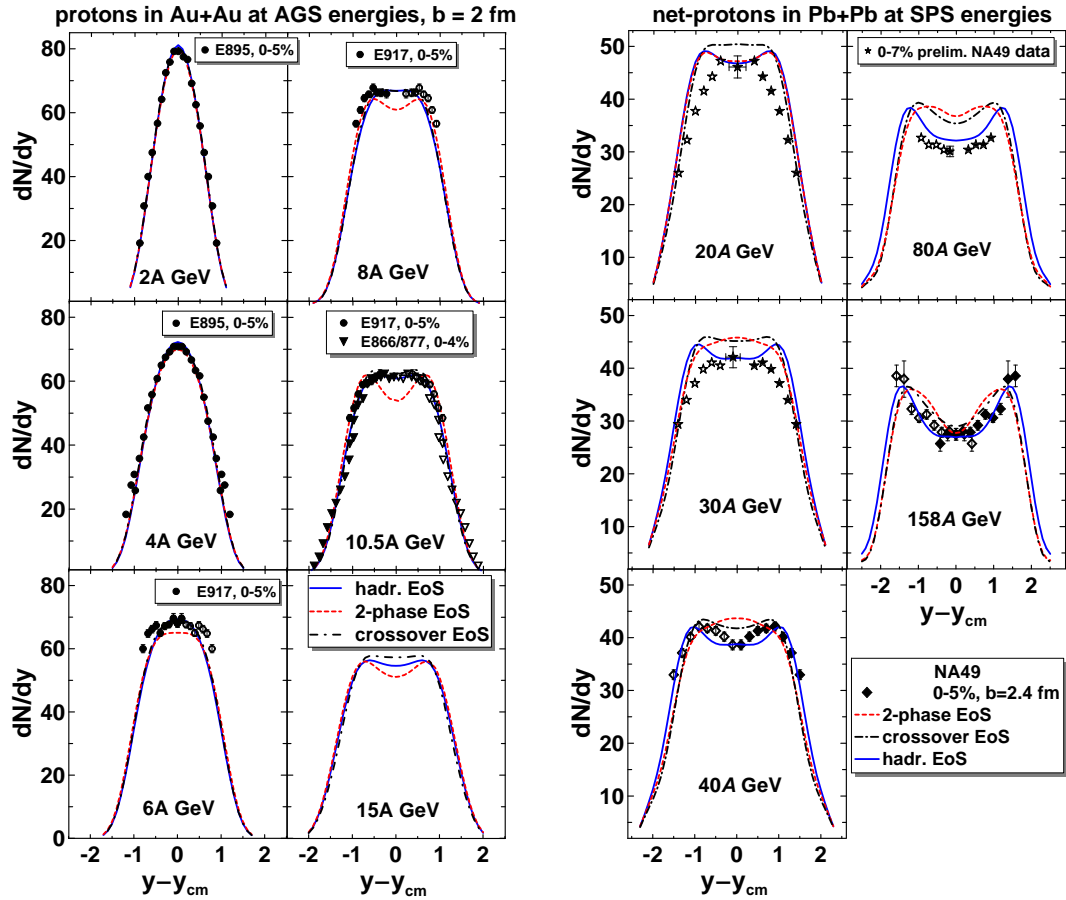


FIG. 2: Rapidity spectra of protons (for AGS energies, see left panel) and net-protons ($p - \bar{p}$) (for SPS energies, see right panel) from central collisions of Au+Au (AGS) and Pb+Pb (SPS). Experimental data are from collaborations E895 [23], E877 [24], E917 [25], E866 [26], and NA49 [27–31]. The percentage shows the fraction of the total reaction cross section, corresponding to experimental selection of central events. Feedback of weak decays into p and \bar{p} yields is disregarded.

similar behavior as that in the 2-phase-EoS scenario: after a plateau or a shallow midrapidity dip at the energy of 8A and 10A GeV, a well pronounced peak at 20A GeV is again observed. However, quantitatively the 2-phase-EoS results certainly disagree with data at 8A GeV, 10A GeV and 40A GeV energies. They also disagree with data 20A GeV and 30A GeV, which however have preliminary status, and hence it is too early to draw any conclusions from comparison with them. The 2-phase-EoS behavior is in contrast with that for the hadronic-EoS scenario, where the form of distribution in central collisions gradually evolve from peak at the midrapidity to a dip. The case of the crossover EoS is intermediate: only a shallow dip occurs at 10A and 15A GeV while at 20A GeV the distribution looks like a plateau.

Predictions of different scenarios diverge to the largest extent in the energy region $8A \text{ GeV} \leq E_{lab} \leq 40A \text{ GeV}$. Unfortunately data at 20A and 30A GeV still have a preliminary status and disagree with any considered scenario. Updated experimental results at energies 20A and 30A GeV are badly needed to pin down the preferable EoS and to check the hint to the zigzag behavior of the

type “peak-dip-peak-dip” in the net-proton rapidity distributions.

IV. ANALYSIS OF “PEAK-DIP-PEAK-DIP” IRREGULARITY

In order to quantify the above-discussed “peak-dip-peak-dip” irregularity, it is useful to make use of the method proposed in Ref. [18]. For this purpose the data on net-proton rapidity distributions are fitted by a simple formula

$$\frac{dN}{dy} = a \left(\exp \left\{ -(1/w_s) \cosh(y - y_{cm} - y_s) \right\} + \exp \left\{ -(1/w_s) \cosh(y - y_{cm} + y_s) \right\} \right) \quad (1)$$

where a , y_s and w_s are parameters of the fit. The form (1) is a sum of two thermal sources shifted by $\pm y_s$ from the midrapidity. The width w_s of the sources can be interpreted as $w_s = (\text{temperature})/(\text{transverse mass})$, if we assume that collective velocities in the sources have no spread with respect to the source rapidities $\pm y_s$. The

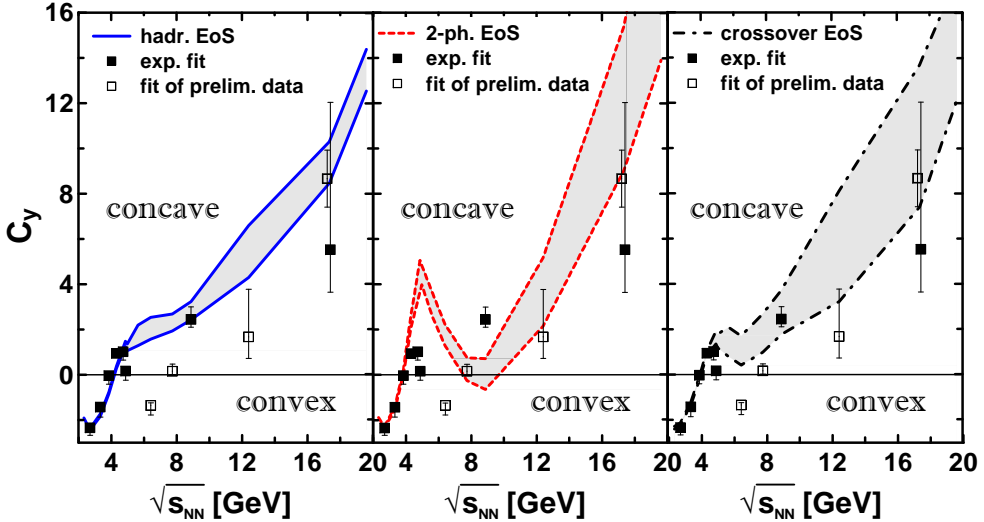


FIG. 3: Midrapidity reduced curvature [see. Eq. (2)] of the (net)proton rapidity spectrum as a function of the center-of-mass energy of colliding nuclei as deduced from experimental data and predicted by 3FD calculations with different EoS's: the hadronic EoS (hadr. EoS) [11] (left panel), the EoS involving a first-order phase transition (2-ph. EoS, middle panel) and the EoS with a crossover transition (crossover EoS, right panel) into the quark-gluon phase [16]. Upper bounds of the shaded areas correspond to fits confined in the region of $|y - y_{cm}|/y_{cm} < 0.7$, lower bounds $-|y - y_{cm}|/y_{cm} < 0.5$.

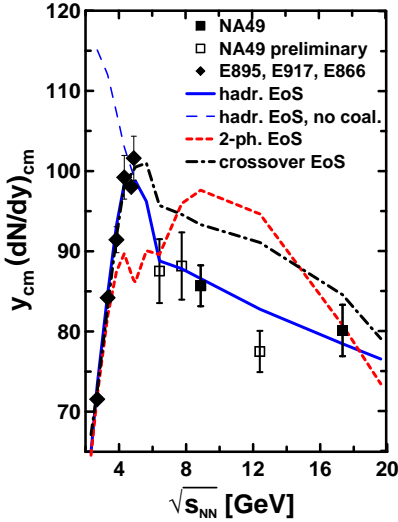


FIG. 4: The same as in Fig. 3 but for midrapidity value of the (net)proton rapidity spectrum scaled by y_{cm} . The thin long-dashed line corresponds to the hadr.-EoS calculation without fragment production, i.e. without coalescence.

parameters of the two sources are identical (up to the sign of y_s) because only collisions of identical nuclei are considered.

The above fit has been done by the least-squares method and applied to both available data and results of calculations. The fit was performed in the rapidity range $|y - y_{cm}|/y_{cm} < 0.7$. The choice of this range is dictated by the data. As a rule, the data are available in this rapidity range, sometimes the data range is even

more narrow (80A GeV and new data at 158A GeV [31]). I put the above restriction in order to treat different data in approximately the same rapidity range. Another reason for this cut is that the rapidity range should not be too wide in order to exclude contribution of cold spectators. The fit in the rapidity range $|y - y_{cm}|/y_{cm} < 0.5$ has been also done in order to estimate uncertainty of the fit parameters associated with the choice of fit range.

A useful quantity, which characterizes the shape of the rapidity distribution, is a reduced curvature of the spectrum at the midrapidity defined as follows

$$C_y = \left(y_{cm}^3 \frac{d^3 N}{dy^3} \right)_{y=y_{cm}} / \left(y_{cm} \frac{dN}{dy} \right)_{y=y_{cm}} = (y_{cm}/w_s)^2 (\sinh^2 y_s - w_s \cosh y_s). \quad (2)$$

The factor $1/(y_{cm} dN/dy)_{y=y_{cm}}$ is introduced in order to get rid of overall normalization of the spectrum. The second part of Eq. (2) presents this curvature in terms of parameters of fit (1). The reduced curvature, C_y , and the midrapidity value, $(y_{cm} dN/dy)_{y=y_{cm}}$, are two independent quantities quantifying the the spectrum in the midrapidity range. Excitation functions of these quantities deduced both from experimental data and from results of the 3FD calculations with different EoS's are displayed in Figs. 3 and 4. Notice that a maximum in $y_{cm}(dN/dy)_{cm}$ at $\sqrt{s_{NN}} = 4.7$ GeV happens only because the light fragment production becomes negligible above this energy. The 3FD calculation without coalescence (i.e. without the light fragment production) reveals a monotonous decrease of $y_{cm}(dN/dy)_{cm}$ beginning from the lowest energy considered here.

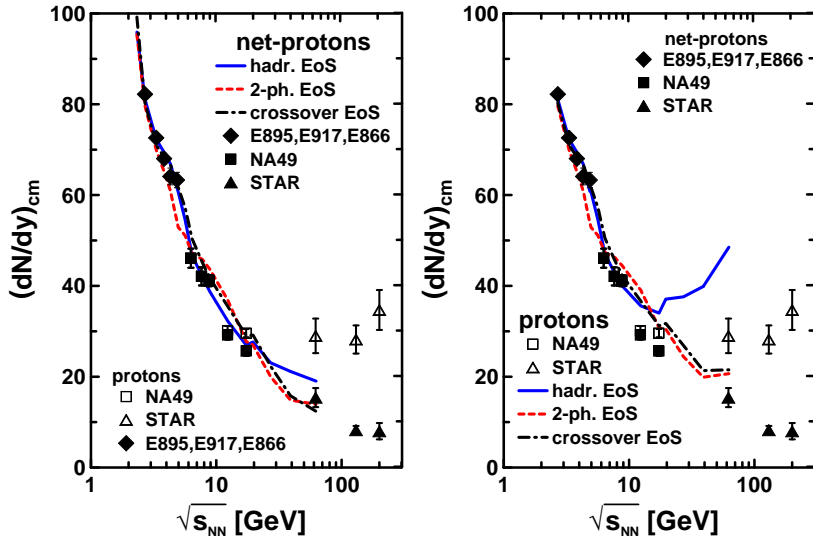


FIG. 5: The same as in Fig. 4 but for midrapidity values of the net-proton (left panel) and proton (right panel) rapidity spectrum in conventional representation, i.e. without scaling. Experimental data are from collaborations E895 [23], E877 [24], E917 [25], E866 [26], NA49 [27–31] and STAR [42].

To evaluate errors of C_y values deduced from data, I estimated the errors produced by the least-squares method, as well as performed fits in different the rapidity ranges: $|y - y_{cm}|/y_{cm} < 0.5$ and $|y - y_{cm}|/y_{cm} < 0.7$, where it is appropriate. Problems were met in fitting the data at 80A GeV [30] and the new data at 158A GeV [31]. These data do not go beyond the side maxima in the rapidity distributions. This results in large uncertainty in the parameters. In particular, because of this problem I keep the old data at 158A GeV [27] in the analysis. The error bars present largest uncertainties among mentioned above. The upper errors of 158A-GeV 80A-GeV points results from the uncertainty of the narrow rapidity range. The uncertainty associated with the choice of the rapidity range turned out to be a dominant one in the case computed data. Therefore, in Fig. 3 results for the computed spectra are presented by shaded areas with borders corresponding to the fit ranges $|y - y_{cm}|/y_{cm} < 0.7$ and $|y - y_{cm}|/y_{cm} < 0.5$. In Fig. 4 the midrapidity values of the rapidity spectra were taken directly from experimental data and calculated results. Therefore, only experimental error bars are displayed there.

Since experimental data at AGS and RHIC energies were taken from Au+Au collisions while at SPS the Pb+Pb collisions were studied, the calculations were performed respectively for Au+Au ($b = 2$ fm) and Pb+Pb ($b = 2.4$ fm) central collisions. In fact, at the same incident energy the computed results for Pb+Pb collisions at $b = 2.4$ fm are very close to those for Au+Au at $b = 2$ fm. Therefore, the corresponding irregularity of the energy dependence of the fit parameters is negligible.

The irregularity in data is distinctly seen here as a zigzag irregularity in the energy dependence of C_y . Of

course, this is only a hint to irregularity since this zigzag is formed only due to preliminary data of the NA49 collaboration. A remarkable observation is that the C_y excitation function in the first-order-transition scenario manifests qualitatively the same zigzag irregularity (left panel of Fig. 3) as that in the data fit, while the hadronic scenario produces purely monotonous behavior. The crossover EoS represents a very smooth phase transition, as mentioned above. Therefore, it is not surprising that it produces only a weak wiggle in C_y .

This zigzag irregularity of the first-order-transition scenario is also reflected in the midrapidity values of the (net)proton rapidity spectrum (Fig. 4). In the conventional representation of the data without multiplying by y_{cm} , the irregularity of the $(dN/dy)_{cm}$ data is hardly visible (Fig. 5). Moreover, the difference between predictions resulted from different EoS's is also scarcely discernible. Thus, the scaled representation of Fig. 4 serves as a zoom revealing differences. In Fig. 5 not only net-protons but also proton midrapidity values are displayed in a wider energy range. However, results for top energy $\sqrt{s_{NN}} = 62.4$ GeV are very approximate, since more accurate computation requires unreasonably high memory and CPU time. As seen, a visible difference between net-protons and proton data, as well between predictions of hadronic EoS and EoS's with phase transitions starts only at RHIC energies. Similar (but based on different, double-gaussian fit) analysis was performed in Ref. [41]. It found no irregularities in excitation functions of the corresponding parameters, in particular, because the analysis of Ref. [41] was restricted to energies $E_{lab} \geq 20$ A GeV.

As it was pointed out in the introduction, the “peak-

dip-peak-dip” irregularity is very natural in a system undergoing a phase transition. First, it is associated with the softest point of a EoS. Therefore, it is not surprising that the irregularity is weaker in the crossover scenario than in the first-order-transition one. Indeed, the softest points in the crossover EoS is less pronounced than in the first-order-transition one [17]. There is no softest point in the hadronic EoS and hence there is no irregularity.

The second reason of this irregularity is a change in the nonequilibrium regime. The 3FD model takes into account the leading nonequilibrium of the nuclear collision associated with a finite stopping power of the nuclear matter. It simulates the finite stopping power by means of friction between three fluids. Naturally, this friction changes when a phase transition happens. In the case of the crossover scenario this change in the friction is very smooth. Therefore, it does not contribute to the irregularity. At the same time this change in the friction enhances the irregularity in the first-order-transition scenario. As it was demonstrated in Ref. [18], if the same friction is used in both phases, the reduced curvature calculated with the 2-phase EoS reveals a wiggle behavior in C_y but with considerably smaller amplitude as compared with zigzag in actual calculations with different frictions in different phases. These different frictions appear quite naturally in the 3FD model. The hadronic friction was estimated in Ref. [20] and works well at lower AGS energies. Therefore, there are no reasons to modify it. The partonic friction, while not microscopically estimated, is fitted to reproduce data at high incident energies. This is a reason to believe that it is a proper choice.

V. CONCLUSION

An irregularity in the baryon stopping is a natural consequence of a phase transition occurring in the compression stage of a nuclear collision. It is a combined effect of the softest point of a EoS and a change in the nonequilibrium regime from hadronic to partonic one. It is important to emphasize that this irregularity is a signal from the hot and dense stage of the nuclear collision.

In order to illustrate this fact, calculations within the 3FD model were performed with three different equations of state, i.e. with a purely hadronic EoS [11], and also with two versions of EoS involving the deconfinement phase transition [16]: an EoS with the first-order phase transition and that with a smooth crossover transition. The crossover transition constructed in Ref. [16] is very smooth. The hadronic fraction survives up to very high energy densities. In this respect, this version of the crossover EoS certainly contradicts results of the lattice QCD calculations, where a fast crossover, at least at zero chemical potential, was found [21]. Therefore, a true EoS is somewhere in between the crossover and 2-phase EoS’s of Ref. [16].

It is found that predictions within the first-order-transition scenario reveal a “peak-dip-peak-dip” irregu-

larity in the incident energy dependence of the form of the net-proton rapidity distributions in central collisions. At low energies, rapidity distributions have a peak at the midrapidity. With the incident energy rise it transforms into a dip, then again into a peak, and with further energy rise the midrapidity peak again change into a dip, which already survives up to arbitrary high energies. The behavior the type of “peak-dip-peak-dip” in central collisions within the 2-phase-EoS scenario is very robust with respect to variation of the model parameters in a wide range. This behavior is in contrast with that for the hadronic-EoS scenario, where the distribution form gradually evolve from peak at the midrapidity to a dip. The case of the crossover EoS is intermediate. Only a weak wiggle of the type of “peak-dip-peak-dip” takes place.

Experimental data also revel a trend of the “peak-dip-peak-dip” irregularity in the energy range $8A$ GeV $\leq E_{lab} \leq 40A$ GeV, which qualitatively similar to that in the first-order-transition scenario while quantitatively differ. However, the this experimental trend is based on preliminary data at energies of $20A$ GeV and $30A$ GeV. In general, predictions of different scenarios diverge to the largest extent in the energy region $8A$ GeV $\leq E_{lab} \leq 40A$ GeV. Therefore, updated experimental results at energies $20A$ and $30A$ GeV are badly needed to pin down the preferable EoS and to check the hint to the zigzag behavior of the type “peak-dip-peak-dip” in net-proton rapidity distributions. Moreover, it would be highly desirable if new data in this energy range are taken within the same experimental setup and at the same centrality selection. Hopefully such data will come from new accelerators FAIR at GSI and NICA at Dubna.

In order to quantify the observed “peak-dip-peak-dip” irregularity, the analysis of the distribution shape proposed in Refs. [18, 19] was applied. This method is based on calculation of the reduced curvature of the spectrum at the midrapidity C_y . In tems of C_y the irregularity in data is distinctly seen as a zigzag irregularity in the energy dependence of C_y . The energy location of this zigzag anomaly coincides with the previously observed anomalies for other hadron-production properties at the low SPS energies [44, 45]. A remarkable observation is that the C_y energy dependence in the first-order-transition scenario manifests qualitatively the same zigzag irregularity, as that in the data fit, though quantitatively does not reproduce the data fit. The hadronic scenario produces purely monotonous behaviour. The crossover EoS represents a very smooth phase transition, as mentioned above. Therefore, it is not surprising that it results in only a weak wiggle in C_y .

Here the distribution of net-baryons was discussed because net-baryons have advantage of being confined by the baryon number conservation. In general, an analysis of the form of particle spectra looks very promising. For instance, in Ref. [43] it was proposed to analyze the incident-energy dependence of the width of pion rapidity distributions. This width can be associated with the sound velocity in the dense stage of the reactions.

It is found that the sound velocity has a local minimum (indicating a softest point in the EoS) in the range of $\sqrt{s_{NN}} = 4\text{-}9$ GeV, which coincides with the range of the “peak-dip-peak-dip” irregularity discussed in this paper and that of the previously observed anomalies for other hadron-production properties [44, 45].

Fruitful discussions with A.V. Merdeev, I.N. Mishustin, L.M. Satarov and D.N. Voskresensky are gratefully

acknowledged. I am grateful to A.S. Khvorostukhin, V.V. Skokov, and V.D. Toneev for providing me with the tabulated 2-phase and crossover EoS’s. The calculations were performed at the computer cluster of GSI (Darmstadt). This work was supported by The Foundation for Internet Development (Moscow) and also partially supported by the Russian Ministry of Science and Education grant NS-215.2012.2.

-
- [1] G. S. F. Stephan, *J. Phys. G* **32**, S447 (2006) [nucl-ex/0607030].
- [2] P. Seyboth [NA49 Collaboration], Addedendum-1 to the NA49 Proposal, CERN-SPSC- 97-26; M. Gazdzicki, nucl-th/9701050; M. Gazdzicki et al. [NA61/SHINE Collaboration], PoS C POD2006, 016 (2006).
- [3] B. Friman, (ed.), C. Hohne, (ed.), J. Knoll, (ed.), S. Leupold, (ed.), J. Randrup, (ed.), R. Rapp, (ed.) and P. Senger, (ed.), *Lect. Notes Phys.* **814**, 1 (2011).
- [4] A. N. Sissakian, A. S. Sorin and V. D. Toneev, *Conf. Proc. C* **060726**, 421 (2006) [nucl-th/0608032].
- [5] A. V. Merdeev, L. M. Satarov and I. N. Mishustin, *Phys. Rev. C* **84**, 014907 (2011) [arXiv:1103.3988 [hep-ph]].
- [6] I. N. Mishustin, A. V. Merdeev and L. M. Satarov, *Phys. Atom. Nucl.* **75**, 776 (2012) [arXiv:1012.4364 [hep-ph]].
- [7] V. N. Russkikh, Yu. B. Ivanov, *Phys. Rev. C* **76**, 054907 (2007) [nucl-th/0611094].
- [8] L. D. Landau and E. M. Lifshitz, “*Fluid Mechanics*” (Pergamon Press, Oxford, 1979).
- [9] C. M. Hung and E. V. Shuryak, *Phys. Rev. Lett.* **75**, 4003 (1995) [hep-ph/9412360].
- [10] Yu. B. Ivanov, V. N. Russkikh, and V.D. Toneev, *Phys. Rev. C* **73**, 044904 (2006) [nucl-th/0503088].
- [11] V. M. Galitsky and I. N. Mishustin, *Sov. J. Nucl. Phys.* **29**, 181 (1979).
- [12] Y. B. Ivanov and V. N. Russkikh, PoS CPOD **07**, 008 (2007) [arXiv:0710.3708 [nucl-th]].
- [13] V. N. Russkikh and Yu. B. Ivanov, *Phys. Rev. C* **74** (2006) 034904 [nucl-th/0606007].
- [14] Yu. B. Ivanov and V. N. Russkikh, *Eur. Phys. J. A* **37**, 139 (2008) [nucl-th/0607070]. *Phys. Rev. C* **78**, 064902 (2008) [arXiv:0809.1001 [nucl-th]].
- [15] Yu. B. Ivanov, I. N. Mishustin, V. N. Russkikh, and L. M. Satarov, *Phys. Rev. C* **80**, 064904 (2009) [arXiv:0907.4140 [nucl-th]].
- [16] A. S. Khvorostukhin, V. V. Skokov, K. Redlich, and V. D. Toneev, *Eur. Phys. J. C* **48**, 531 (2006) [nucl-th/0605069].
- [17] E. G. Nikonov, A. A. Shanenko and V. D. Toneev, *Heavy Ion Phys.* **8**, 89 (1998) [nucl-th/9802018].
- [18] Yu. B. Ivanov, *Phys. Lett. B* **690**, 358 (2010) [arXiv:1001.0670 [nucl-th]].
- [19] Y. B. Ivanov, *Phys. At. Nucl.* **75** 621 (2012) [1101.2092 [nucl-th]].
- [20] L. M. Satarov, *Yad. Fiz.* **52**, 412 (1990) [Sov. J. Nucl. Phys. **52**, 264 (1990)].
- [21] Y. Aoki, G. Endrodi, Z. Fodor, S. D. Katz and K. K. Szabo, *Nature* **443**, 675 (2006) [hep-lat/0611014].
- [22] I. C. Arsene, L. V. Bravina, W. Cassing, Yu. B. Ivanov, A. Larionov, J. Randrup, V. N. Russkikh, V. D. Toneev, G. Zeeb, D. Zschiesche, *Phys. Rev. C* **75**, 034902 (2007) [nucl-th/0609042].
- [23] J. L. Klay *et al.* [E-0895 Collaboration], *Phys. Rev. C* **68**, 054905 (2003) [nucl-ex/0306033].
- [24] J. Barrette *et al.* (E877 Collab.), *Phys. Rev. C* **62**, 024901 (2000).
- [25] B. B. Back *et al.*, (E917 Collab.), *Phys. Rev. Lett.* **86**, 1970 (2001).
- [26] J. Stachel, *Nucl. Phys.* **A654**, 119c (1999) [nucl-ex/9903007].
- [27] H. Appelshäuser *et al.* (NA49 Collab.), *Phys. Rev. Lett.* **82**, 2471 (1999).
- [28] T. Anticic *et al.* (NA49 Collab.), *Phys. Rev. C* **69**, 024902 (2004).
- [29] C. Alt *et al.* (NA49 Collab.), *Phys. Rev. C* **73**, 044910 (2006) [nucl-ex/0512033].
- [30] C. Blume (NA49 Collab.), *J. Phys. G* **34**, S951 (2007) [nucl-ex/0701042].
- [31] T. Anticic *et al.* [NA49 Collaboration], *Phys. Rev. C* **83**, 014901 (2011) [arXiv:1009.1747 [nucl-ex]].
- [32] C. Alt *et al.* [NA49 Collaboration], *Phys. Rev. C* **68**, 034903 (2003) [nucl-ex/0303001].
- [33] W. Cassing and E. L. Bratkovskaya, *Nucl. Phys.* **A831**, 215 (2009) [arXiv:0907.5331 [nucl-th]].
- [34] J. Steinheimer V. Dexheimer, H. Petersen, M. Bleicher, S. Schramm, and H. Stoecker, *Phys. Rev. C* **81**, 044913 (2010) [arXiv:0905.3099 [hep-ph]].
- [35] E. L. Bratkovskaya, M. Bleicher, M. Reiter, S. Soff, H. Stoecker, M. van Leeuwen, S. A. Bass, and W. Cassing, *Phys. Rev. C* **69**, 054907 (2004) [nucl-th/0402026].
- [36] H. Weber, E. L. Bratkovskaya, W. Cassing, and H. Stöcker, *Phys. Rev. C* **67**, 014904 (2003) [nucl-th/0209079].
- [37] H. Weber, E. L. Bratkovskaya, and H. Stoecker, *Phys. Rev. C* **66**, 054903 (2002).
- [38] A. B. Larionov, O. Buss, K. Gallmeister, and U. Mosel, *Phys. Rev. C* **76**, 044909 (2007) [arXiv:0704.1785 [nucl-th]].
- [39] M. Wagner, A. B. Larionov, and U. Mosel, *Phys. Rev. C* **71**, 034910 (2005) [nucl-th/0411010].
- [40] A. Andronic, P. Braun-Munzinger and J. Stachel, *Nucl. Phys. A* **772**, 167 (2006) [nucl-th/0511071].
- [41] Y. Mehtar-Tani and G. Wolschin, *Europhys. Lett.* **94**, 62003 (2011) [arXiv:1102.3134 [hep-ph]].
- [42] B. I. Abelev *et al.* [STAR Collab.], *Phys. Rev. C* **79**, 034909 (2009) [arXiv:0808.2041 [nucl-ex]].
- [43] J. Steinheimer and M. Bleicher, *Eur. Phys. J. A* **48**, 100 (2012) [arXiv:1207.2792 [nucl-th]].
- [44] C. Alt *et al.* [NA49 Collab.], *Phys. Rev. C* **77**, 024903 (2008).
- [45] M. Gazdzicki and M. I. Gorenstein, *Acta Phys. Polon. B* **30**, 2705 (1999).